

Electron correlations and charge density wave in the topological kagome metal FeGe

Chandan Setty^{⊕,†,1}, Christopher A. Lane^{⊕,2}, Lei Chen,¹ Haoyu Hu,¹ Jian-Xin Zhu,² and Qimiao Si¹

¹*Department of Physics & Astronomy, Rice Center for Quantum Materials, Rice University, Houston, Texas 77005, USA*

²*Theoretical Division, Los Alamos National Laboratory, Los Alamos, New Mexico 87545 USA*

Charge order in kagome metals is of extensive current interest. Recently, a charge density wave was discovered in the *magnetic* binary kagome metal FeGe [1]. In analogy to its predecessor, the non-magnetic AV_3Sb_5 ($A=K, Cs, Rb$), the in-plane ordering occurs at the M point. In contrast, however, the system manifestly shows effects of substantial correlations. Here we identify the topological bands crossing the Fermi energy (E_F) in FeGe and characterize the correlation-induced renormalization of these bands. We then derive a charge order from an effective model comprising topological kagome ‘flat’ bands in the presence of a magnetic order. We demonstrate edge states as well as excess out-of-plane magnetic moment associated with the charge order; both are fingerprints of non-trivial band topology and consistent with recent experimental observations. Our results point to FeGe as an ideal platform to realize and elucidate correlated topological physics.

Introduction: Charge order phases in kagome metals have garnered much recent attention owing to their highly unconventional properties. Especially in the vanadium based non-magnetic ternary kagome materials (AV_3Sb_5 ; $A=K, Cs, Rb$) [2–4], charge order has been found [5–11] and shows several non-trivial characteristics. These include the breaking of time-reversal (T) symmetry [12–14], anomalous Hall transport [15], nematicity [14, 16] and other accompanying/competing orders [8, 10, 17, 18], and possible coexistence with unconventional superconductivity [19].

Another prominent class of transition element kagome metals is the binary T_mX_n ($T=Fe, Co, Ni$ and $X=Ge, Sn$). They have magnetic ground states [20–24] and possess flat bands near the Fermi level (E_F) [21, 25, 26]. Recently hexagonal FeGe (SG 191, $P6/mmm$) was shown to be the first member in this family ($T_m \sim 400$ K [27]) where charge order is identified, with a transition temperature of $T_{CO} \sim 110$ K [1, 28, 29]. The spins are aligned (anti-)ferromagnetically (between) within the kagome planes and point in a direction perpendicular to the layers [27].

Much of the currently known phenomenology of the charge order is analogous to the ternary compounds – the in-plane ordering occurs at M point (2×2 order) and the STM peaks are sensitive to the directionality of the applied perpendicular (c -axis) magnetic field. However, in contrast with the ternary family, here the charge order emerges from a magnetic parent phase [1], and is accompanied by edge states [28] and an excess contribution to the ordered magnetic moment [1] below T_{CO} .

In this work we develop a model of charge order in FeGe. We identify two minimal ingredients – the presence of flat bands crossing E_F and their non-trivial topology – that can broadly capture much of the observed data. We justify the relevance of these two ingredients to FeGe using first principle calculations. To isolate the salient physics from the complexities of the real-material electronic structure, we begin from an extended Hubbard model on a kagome lattice. We then seek a low energy

model for the topological flat bands by working in the limit where Coulomb interactions are comparable to the bandwidth of the flat bands. By solving the low-energy model non-perturbatively using the slave-spin method, we analyze the nature of the resulting charge order phase with focus on the role played by the parent magnetic phase. We find that the non-trivial band topology of the kagome lattice, and its interplay with charge order and magnetism give rise to topological edge states in the charge order gap. Another key result we uncover is an excess magnetic moment, which points along the existing magnetic order, arising from the intertwining of charge and spin degrees of freedom – a property unique to correlated phases derived from topological bands [30]. Thus we identify previously unknown fingerprints of non-trivial band topology manifest in correlated phases.

Our strategy is to isolate a pair of flat bands crossing E_F with chern numbers ± 1 that are split by the internal field of the parent magnetic phase. To write an effective model with interactions for this pair of ‘active’ bands, we follow the framework developed by several of us in Ref. [30] where such a charge order was already predicted for binary kagome metals. Wannier construction of exponentially localized wannier orbitals (WOs) [31–34] allows for tight binding description of the low energy topological bands, from which we can study the correlation effect.

Topological bands: Before describing the minimal interacting model, we discuss the electronic structure of FeGe and its corresponding topological characteristics. Fig. 1 (top row) shows the spin-orbit coupled bands, calculated by density-functional theory (DFT), in the non-magnetic (NM) (left panel) and magnetic (right panel) phases respectively. In both the nonmagnetic phase (SG $P6/mmm$) and the magnetic one (SG $P6/m'm'm'$), the flat bands directly cross E_F .

Fig. 2 (top left) highlights three topological bands near E_F in the NM phase with spin-orbit coupling (SOC) in green, red and purple. The topological indices for these band pairs appear in Fig. 2 (top right).

Electron correlations and DMFT calculations: FeGe

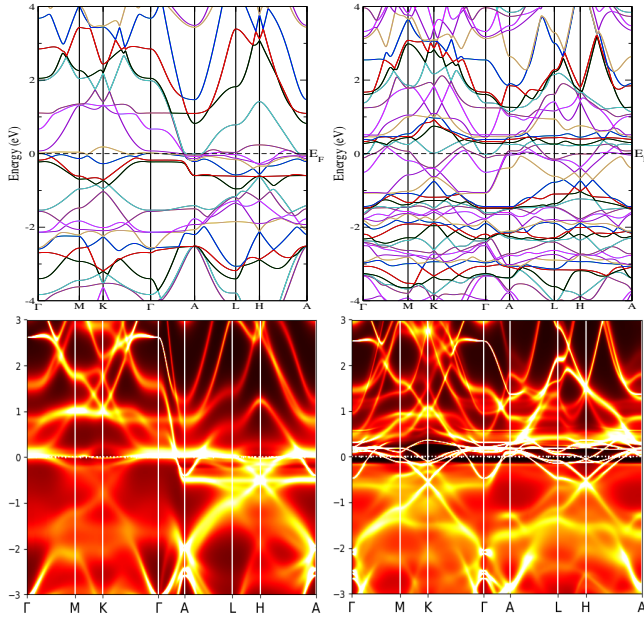


FIG. 1. (Top row) First principles band structure of FeGe in the nonmagnetic (left) and magnetic (right) phases with SOC. (Bottom row) Same as top row but with Coulomb interactions ($U = 4$ eV) accounted for through DMFT.

shows the effect of substantial electron correlations [1]. It has a relatively large room temperature resistivity, $\sim 160\mu\Omega\cdot\text{cm}$, which reaches the Mott-Ioffe-Regel value, implicating FeGe as a bad metal. The electronic bands also show substantial correlation-induced renormalization [1, 29]. We characterize this correlation effect using dynamical mean field theory (DMFT). The DFT+DMFT [35, 36] results are shown in the bottom row in Fig. 1. The flat bands become very narrow and the spectral weight is highly concentrated at E_F in both the NM and magnetic phases. See also Supplemental Material (SM) Fig. 5.

Importantly, the topologically non-trivial flat bands still cross E_F . The density of states (DOS) near E_F are completely dominated by the flat bands in both the NM and magnetic phases. This is highlighted by black arrows in Fig. 2 (bottom left). The conclusion stands in the presence of interactions as seen in DMFT (bottom right panel of Fig. 2).

Effective model for correlated topological bands: Having provided evidence for the existence of topological flat bands crossing E_F , we now utilize the minimal ingredients to study correlation-driven charge order. As a proof-of-principle demonstration, we focus on the intralayer couplings within a kagome layer. The minimal total Hamiltonian in the physical electron basis (UV limit) is given as $\mathcal{H} = \mathcal{H}_0 + \mathcal{H}_1$. The kinetic part \mathcal{H}_0 is described by electrons hopping on a kagome lattice in the presence of a Zeeman field of the magnetic order within the plane

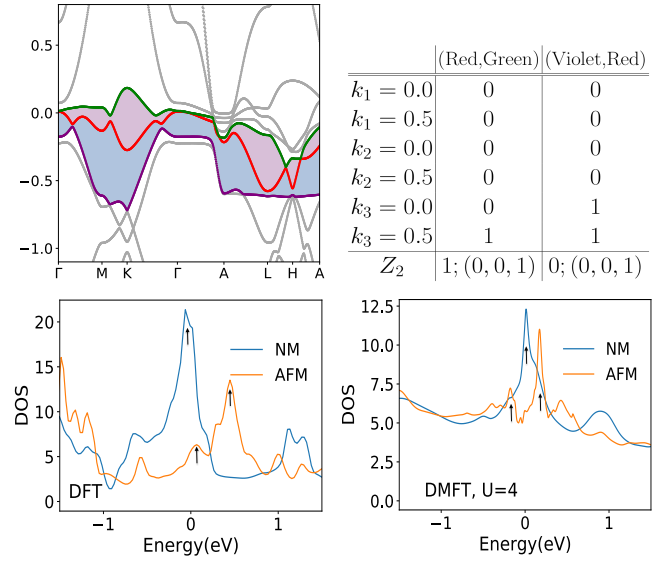


FIG. 2. (Top left) The three topological bands near E_F in the NM phase where the gaps are shaded in blue and red, (top right) Z_2 number for each of the six time reversal invariant planes and resulting Z_2 topological index for the (green, red) and (violet,red) pair of bands as shown in the top left panel. (Bottom left) DOS in the NM and magnetic phases without interactions and (Bottom right) DOS results from DMFT. The black arrows indicate flat band contributions to DOS.

and is written as

$$\begin{aligned}
 \mathcal{H}_0 = & -t \sum_{\langle ij \rangle \alpha \beta} c_{i\alpha}^\dagger c_{j\beta} + i\lambda_1 \sum_{\langle ij \rangle \alpha \beta} (\mathbf{E}_{ij} \times \mathbf{R}_{ij}) \cdot c_{i\alpha}^\dagger \sigma c_{j\beta} \\
 & -t_2 \sum_{\langle\langle ij \rangle\rangle \alpha \beta} c_{i\alpha}^\dagger c_{j\beta} + i\lambda_2 \sum_{\langle\langle ij \rangle\rangle \alpha \beta} (\mathbf{E}_{ij} \times \mathbf{R}_{ij}) \cdot c_{i\alpha}^\dagger \sigma c_{j\beta} \\
 & + h \sum_{i\alpha} c_{i\alpha}^\dagger \sigma_z c_{i\alpha}.
 \end{aligned} \quad (1)$$

Here $c_{j\alpha}^\dagger$ creates an electron at site j and internal quantum number α . The internal quantum numbers include both sub-lattice and spin indices. t, t_2 and $\lambda_{1,2}$ are the hopping and SOC parameters for the nearest neighbor and next-nearest neighbor lattice sites respectively. The displacement from site i to site j is \mathbf{R}_{ij} , and the electric field experienced by the electrons along \mathbf{R}_{ij} is \mathbf{E}_{ij} . The last term arises due to the Zeeman field experienced by the electrons from the magnetic moments pointed out-of-plane in a quasi 2D kagome plane. We assume this field to be uniform and proportional to h . Fig. 3 (left panel) describes the lattice structure and magnetically ordered moments. The interaction part, \mathcal{H}_1 , is given by the extended Hubbard term on the kagome lattice

$$\mathcal{H}_1 = \sum_{ij\alpha\beta} U_{j,\alpha\beta} n_{i\alpha} n_{i+\beta} \quad . \quad (2)$$

It contains the onsite Hubbard interaction U , and nearest and next-nearest neighbor density interactions V and V'

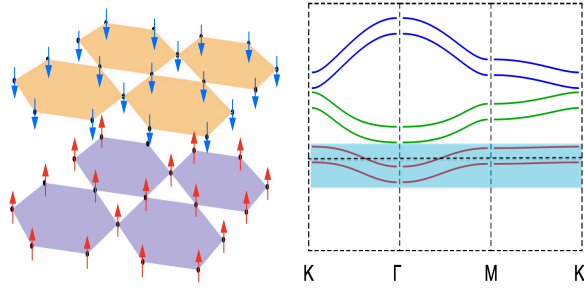


FIG. 3. (Left) The kagome lattice of FeGe in the magnetic phase with ferromagnetic in-plane and anti-ferromagnetic out-of-plane moments. (Right) Band structure in the presence of spin-orbit coupling with the 'active' topological bands near E_F (dashed line) marked in blue.

respectively. For convenience, these parameters are succinctly expressed in terms of $U_{j,\alpha\beta}$ and the corresponding number operators are denoted by $n_{i\alpha}$. We use the primitive vectors of the triangular lattice $\mathbf{n}_1 = 2a(\frac{1}{2}, \frac{\sqrt{3}}{2})$, $\mathbf{n}_2 = 2a(-\frac{1}{2}, \frac{\sqrt{3}}{2})$, $\mathbf{n}_3 = 2a(1, 0)$ where a is the nearest neighbor inter atomic spacing, to write the minimal band structure from the kinetic Hamiltonian Eq. 1. The non-interacting bands of the minimal model are shown in Fig. 3 (right panel). There are three pairs of bands separated in energy and each is split by the Zeeman field. Each pair has chern numbers $C = \pm 1, 0, \pm 1$ from highest to lowest energy. Note that the total chern number for each pair of bands sums to zero even the presence of the Zeeman field [37].

To mimic the realistic electronic structure of FeGe, we place the chemical potential in the lowest pair of flat bands with $C = \pm 1$ as highlighted in the blue region in Fig. 3 (right panel). We seek a low energy model describing this pair of bands. To this end, we wannierize the bands to derive exponentially localized WOs [30–32]. Denoting $b_{i\mu}^\dagger$ as the creation operator in the WO basis on site i , the low energy (IR) Hamiltonian obtained after projecting on the bands crossing E_F is written as $H = H_0 + H_I$ where

$$H_0 = \sum_{ij} \sum_{\mu\nu} b_{i\mu}^\dagger t_{ij}^{\mu\nu} b_{j\nu}$$

$$H_I = \sum_{ijkl} \sum_{m\mu\nu} u_{\mu\mu'\nu\nu'}(j, k, l) b_{i\mu}^\dagger b_{i+j\nu'} b_{i+k\nu}^\dagger b_{i+l\nu} \quad (3)$$

Here $t_{ij}^{\mu\nu}$ and $u_{\mu\mu'\nu\nu'}(j, k, l)$ are respectively the hopping parameters (see SM Table I and SM Fig. 8) and interaction matrix elements. The interaction parameters are listed in the SM (Tables I-III) of Ref. [30]. It is noteworthy that the interaction parameters $u_{\mu\mu'\nu\nu'}(j, k, l)$ are strictly non-local with no onsite interactions. This is because the wannierization procedure splits the WO centers in real space (See Fig.1(b) of [30]). This lack of a common wannier center arises from the $C = \pm 1$ chern distribution and is hence an intrinsic topological prop-

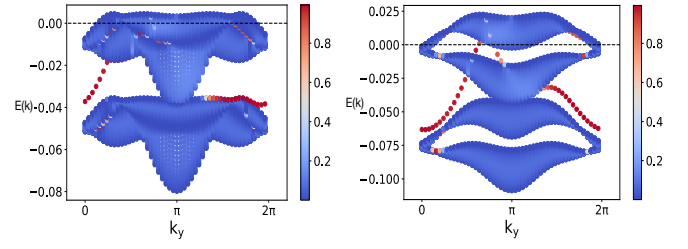


FIG. 4. Edge states with the chemical potential located in the upper sub-band and a gapless bulk spectrum. The color scale marks the spectral weight of the states. (Left panel) Edge states in the parent magnetic order. (Right panel) Edge states in the charge order phase derived from magnetic order.

erty. A key consequence of the wannier center split is the coupling of charge and spin degrees of freedom and is ultimately responsible for the enhanced T -symmetry breaking upon entry into the charge order state [30].

A full analysis of the Hamiltonian in Eq. 3 without the magnetic order appears in Ref. [30]. We have explicitly checked that a similar analysis in the presence of a Zeeman term due to the magnetic order yields an analogous phase diagram with the phase boundaries modified only quantitatively. Above a critical next nearest neighbor interaction V' , a correlation driven charge order phase at the M point in the Brillouin zone (BZ) is stable. This order is interesting since, for trivial bands, the two WOs share the same Wannier center and a minimization of the onsite Coulomb repulsion would have yielded a spin order. Instead, in our case, the non-local V' interaction dominates and drives a charge order at M .

The charge order also couples to an applied perpendicular magnetic field due to the topology driven mixing between the charge and spin order consistent with recent STM data [28]. For further details regarding these conclusions, we refer the reader to Ref. [30]. For the purposes of the current work, we focus on the edge states and enhanced moment in the charge order phase. Here, the Hamiltonian in the $c_{\mathbf{k}\alpha\sigma}$ basis takes the form

$$H = \sum_{\mathbf{k}, \alpha, \gamma} \left[c_{\mathbf{k}, \alpha, \uparrow}^\dagger [h_{0, \mathbf{k}}]_{\alpha\gamma} c_{\mathbf{k}, \gamma, \uparrow} + c_{\mathbf{k}, \alpha, \downarrow}^\dagger [h_{0, -\mathbf{k}}^*]_{\alpha\gamma} c_{\mathbf{k}, \gamma, \downarrow} \right]$$

$$+ \sum_{\mathbf{k}, \alpha} h_0 (c_{\mathbf{k}, \alpha, \uparrow}^\dagger c_{\mathbf{k}, \alpha, \uparrow} - c_{\mathbf{k}, \alpha, \downarrow}^\dagger c_{\mathbf{k}, \alpha, \downarrow}) \quad (4)$$

$$+ \sum_{\mathbf{k}, \alpha, \gamma, \sigma, \sigma'} \left[\sum_a \phi_{\mathbf{Q}}(u_{\mathbf{k}+\mathbf{Q}, \alpha, \sigma}^a)^* u_{\mathbf{k}, \gamma, \sigma'}^a \right] c_{\mathbf{k}+\mathbf{Q}, \alpha, \sigma}^\dagger c_{\mathbf{k}, \gamma, \sigma'}$$

where α, γ denotes sublattice indices. $h_{0, \mathbf{k}}$ is the hopping matrix of spin up electron with bare dispersions $\epsilon_{\mathbf{k}}, \epsilon_{\mathbf{k}+\mathbf{Q}}$ and h_0 is the magnetic field. $\phi_{\mathbf{Q}}$ denotes the charge order parameter in the wannier-orbital basis which is a real number. $u_{\mathbf{k}, \alpha, \sigma}^a$ is the wavefunction of WO a , defined as $b_{a, \mathbf{k}} = \sum_{\alpha, \sigma} u_{\mathbf{k}, \alpha, \sigma} c_{\mathbf{k}, \alpha, \sigma}$, and is related to the Haldane matrix as described in Ref. [30].

The terms that mix two opposite spins σ and $\bar{\sigma}$ (Eq. 4, with a finite momentum \mathbf{Q}) couple charge and spin. They would not have existed for charge order from topologically trivial bands when the SOC is directed out of the kagome plane. The uniqueness of such terms to correlated orders derived from topological bands is due to wannier center splitting discussed above [30]. This effect will be crucial for understanding the charge order-induced magnetic moment appearing later.

We can now obtain edge states by solving Eq. 4 on a slab. Fig. 4 shows a plot of the edge state spectrum along the $x = 0$ edge in the reduced BZ. The spectral intensities are shown in a color scale. The left (right) panel corresponds to the edge state spectrum in the parent magnetic order (charge order) phase. Whereas the edge states connecting the top and bottom sub-bands are overwhelmed by the gapless bulk bands in the magnetic parent phase, they completely dominate in the charge order phase. Additional edge state analysis when the bulk is fully gapped by the Zeeman field appears in the SM Fig. 7. The origin of the edge state behavior is tied to the non-zero chern numbers of the kagome flat bands crossing E_F and a non-trivial coupling between the magnetic and charge orders. The out-of-plane field of the magnetic order splits the non-interacting bands with equal and opposite chern numbers and the low energy (non-interacting) model written in the original c electron basis can be mapped to the Haldane bands. Hence the suppression of the density of states at the chemical potential due to the charge order enables the observation of edge states as observed in STM [28].

We now illustrate our topological mechanism for the enhanced magnetic moment, at the in-plane $\mathbf{q} = 0$, along the positive c -axis in the charge ordered phase. We do this by expanding Eq. 4 in a Ginzburg-Landau type of free energy in terms of the charge order parameters $\Delta_{\mathbf{Q}} \sim \sum_{\mathbf{k}} \langle c_{\mathbf{k}\alpha\uparrow}^\dagger c_{\mathbf{k}+\mathbf{Q}\alpha\downarrow} \rangle$ and $\Delta'_{\mathbf{Q}} \sim \sum_{\mathbf{k}} \langle c_{\mathbf{k}+\mathbf{Q}\alpha\uparrow}^\dagger c_{\mathbf{k}\alpha\downarrow} \rangle$. For a single sub-lattice α , this is given as

$$F[\Delta_{\mathbf{Q}_i}, \Delta'_{\mathbf{Q}_i}] = F_0[\Delta_{\mathbf{Q}_i}, \Delta'_{\mathbf{Q}_i}] + \Delta F[\Delta_{\mathbf{Q}_i}, \Delta'_{\mathbf{Q}_i}] \quad (5)$$

$$\Delta F[\Delta_{\mathbf{Q}_i}, \Delta'_{\mathbf{Q}_i}] = -h'\gamma \sum_i \left(\Delta_{\mathbf{Q}_i} \Delta_{-\mathbf{Q}_i} + \Delta'_{\mathbf{Q}_i} \Delta'_{-\mathbf{Q}_i} \right).$$

Here F_0 is independent of a ‘probe’ field h' (SM, Eq. 10), and $\gamma \simeq \frac{3h_0}{2T_{CO}^4} \left[\frac{-1+\tilde{h}_0^{-1} \sinh \tilde{h}_0}{\tilde{h}_0^2(1+\cosh \tilde{h}_0)} \right]$ with $\tilde{h}_0 = h_0/T_{CO}$ in the nested, flat band limit of $\epsilon_{\mathbf{k}} = \epsilon_{\mathbf{k}+\mathbf{Q}_i} \sim 0$. \mathbf{Q}_i are the M point wave vectors corresponding to the 2×2 charge order. The ΔF term (see SM Fig. 9) couples charge and $\mathbf{Q} = 0$ magnetic orders and is odd in the static and probe fields h_0 and h' . The induced magnetic moment becomes

$$\delta M = -\frac{\partial F[\Delta_{\mathbf{Q}_i}]}{\partial h'} \propto \gamma (\Delta_{\mathbf{Q}_i} \Delta_{-\mathbf{Q}_i} + \Delta'_{\mathbf{Q}_i} \Delta'_{-\mathbf{Q}_i}). \quad (6)$$

From the expression of γ above, the induced δM is *along* the direction of the static magnetic field (h_0) and rises quadratically in the order parameter upon entry into the

charge order phase. This result is consistent with neutron scattering data [1].

As alluded to earlier, the terms proportional to γ in Eqs. 5, 6 have a topological origin. From the definitions of $\Delta_{\mathbf{Q}}$ and $\Delta'_{\mathbf{Q}}$, it is evident that the order parameters have a finite wave vector and mix opposite spins, hence coupling spin and charge. This is absent for charge order derived from trivial bands with an out-of-plane SOC. In fact, the finite wave vector non-spin flip terms of the type $\sum_{\mathbf{k}} \langle c_{\mathbf{k}+\mathbf{Q}\alpha\sigma}^\dagger c_{\mathbf{k}\alpha\sigma} \rangle$ do not pin the induced magnetic moment to h_0 . Hence the induced δM *along* the static h_0 is a fingerprint of topology of the parent magnetic phase.

Discussion: Several points are in order. While the suppression of the DOS close to the chemical potential due to the charge order enables the observation of edge states in STM, it should be noted that the bulk states need not be fully gapped or even nodal for the observation of edge states. Even a modest suppression of the spectral weight at $E_F - 30\% - 40\%$ of the high temperature value with a large residual density of states – is sufficient for the edge spectrum to be discernible. This is consistent with our calculations in Figs 4 where edge states have a large spectral weight despite the lack of a full gap in the charge order phase.

In principle, such topological edge states should exist in the purely magnetic phase as well ($T_{CO} < T < T_m$). However, both DFT and DMFT demonstrate large density of states of the bulk bands near E_F in this regime. Correspondingly, edge states are expected to be smeared by the bulk bands crossing E_F . This picture is supported by our calculations in Fig. 4. In fact, topological surface states are expected to exist even in the normal state above T_m due to the non-trivial topology of the bands, albeit mixed with the more dominant bulk states. Recently such states were observed in photoemission measurements of the ternary kagome compounds [11] in both the normal and charge ordered phases.

We have delineated the role of van Hove singularities in the electronic structure. They are located $\sim -0.6eV$ below E_F in the nonmagnetic phase, and are pushed closer to E_F in the magnetic phase. However, the flat bands always dominate the DOS. As seen in the bottom panels Fig. 1, and further highlighted in SM (Fig. 6), the density of states (DOS) from the van Hove singularities is essentially completely obscured by the topological flat bands. This renders the possibility of a strong coupling topological mechanism for the charge order more viable and robust [30]. Finally, we have illustrated the topological mechanism by focusing on an effective model with only intra-layer coupling. Generalization of our analysis to the more realistic 3D case is left for future investigations.

In conclusion, the recent discovery of charge order in the topological flat band magnetic kagome metal FeGe opens up a new platform for exploring flat band correlated phases and their topological properties. While the charge order in FeGe shares many features with its

ternary counterparts AV_3Sb_5 ($A = K, Cs, Rb$), it is also distinct in important ways. The strong correlation driven band renormalizations, active topological flat bands, appearance of edge states, and enhancement of the magnetic moments below the charge ordering temperature are a few key aspects unique to FeGe. Beyond what was discussed in the nonmagnetic setting [30], namely correlation driven charge order, ordering at the wavevector M in the BZ, and breaking of time-reversal symmetry, we have shown here that our minimal model in a magnetic setting provides a qualitative understanding of the most salient and puzzling features of the charge order in FeGe: (i) the existence of edge states and (ii) development of an excess magnetic moment with the in-plane $\mathbf{q} = 0$. The origin of all these exotic properties can be traced to the non-trivial band topology of the magnetic parent phase. As such, our results will likely have general implications on the interplay of topology and correlations in a broad range of correlated systems.

Acknowledgements: We thank P. C. Dai, M. Yi, J. X. Yin for sharing their results with us and for useful discussions. This work has in part been supported by the AFOSR under Grant No. FA9550-21-1-0356 (C.S. and Q.S.) and the Robert A. Welch Foundation Grant No. C-1411 (L. C. and H.H.). Work at Los Alamos was supported by LANL LDRD Program, UC Laboratory Fees Research Program (Grant Number: LFR-20-653926), and in part by Center for Integrated Nanotechnologies, a U.S. DOE BES user facility. One of us (Q.S.) acknowledges the hospitality of the Aspen Center for Physics, which is supported by NSF grant No. PHY-1607611.

⊕ These authors contributed equally to this work.

† Email: csetty@rice.edu

-
- [1] Xiaokun Teng, Lebing Chen, Feng Ye, Elliott Rosenberg, Zhaoyu Liu, Jia-Xin Yin, Yu-Xiao Jiang, Ji Seop Oh, Zahid Hasan, Kelly Neubauer, Bin Gao, Yaofeng Xie, Makoto Hasimoto, Donghui Lu, Chris Jozwiak, Aaron Bostwick, Eli Rotenberg, Robert Birgeneau, Jiun-Haw Chu, Ming Yi, and Pengcheng Dai, “Discovery of charge density wave in a correlated kagome lattice antiferromagnet,” Submitted (2022).
- [2] Brenden R Ortiz, Lídia C Gomes, Jennifer R Morey, Michal Winiarski, Mitchell Bordelon, John S Mangum, Iain WH Oswald, Jose A Rodriguez-Rivera, James R Neilson, Stephen D Wilson, *et al.*, “New kagome prototype materials: discovery of kv 3 sb 5, rbv 3 sb 5, and csv 3 sb 5,” *Physical Review Materials* **3**, 094407 (2019).
- [3] Brenden R Ortiz, Samuel ML Teicher, Yong Hu, Julia L Zuo, Paul M Sarte, Emily C Schueller, AM Milinda Abeykoon, Matthew J Krogstad, Stephan Rosenkranz, Raymond Osborn, *et al.*, “Cs v 3 sb 5: A z 2 topological kagome metal with a superconducting ground state,” *Physical Review Letters* **125**, 247002 (2020).
- [4] Brenden R Ortiz, Paul M Sarte, Eric M Kenney, Michael J Graf, Samuel ML Teicher, Ram Seshadri, and Stephen D Wilson, “Superconductivity in the z 2 kagome metal kv 3 sb 5,” *Physical Review Materials* **5**, 034801 (2021).
- [5] Yu-Xiao Jiang, Jia-Xin Yin, M Michael Denner, Nana Shumiya, Brenden R Ortiz, Junyi He, Xiaoxiong Liu, Songtian S Zhang, Guoqing Chang, Ilya Belopolski, *et al.*, “Unconventional chiral charge order in kagome superconductor kv3sb5,” *Nature Materials* **20**, 1353 (2021).
- [6] He Zhao, Hong Li, Brenden R Ortiz, Samuel ML Teicher, Taka Park, Mengxing Ye, Ziqiang Wang, Leon Balents, Stephen D Wilson, and Ilija Zeljkovic, “Cascade of correlated electron states in a kagome superconductor csv3sb5,” *Nature* (2021), <https://doi.org/10.1038/s41586-021-03946-w>.
- [7] Xiaoxiang Zhou, Yongkai Li, Xinwei Fan, Jiahao Hao, Yaomin Dai, Zhiwei Wang, Yugui Yao, and Hai-Hu Wen, “Origin of the Charge Density Wave in the Kagome Metal CsV_3Sb_5 as Revealed by Optical Spectroscopy,” arXiv e-prints, arXiv:2104.01015 (2021), arXiv:2104.01015 [cond-mat.supr-con].
- [8] Zuowei Liang, Xingyuan Hou, Wanru Ma, Fan Zhang, Ping Wu, Zongyuan Zhang, Fanghang Yu, J-J Ying, Kun Jiang, Lei Shan, *et al.*, “Three-dimensional charge density wave and robust zero-bias conductance peak inside the superconducting vortex core of a kagome superconductor csv 3 sb 5,” arXiv preprint arXiv:2103.04760 (2021).
- [9] E Uykur, BR Ortiz, SD Wilson, M Dressel, and AA Tsirlin, “Optical detection of charge-density-wave instability in the non-magnetic kagome metal kv 3 sb 5,” arXiv preprint arXiv:2103.07912 (2021).
- [10] HX Li, TT Zhang, Y-Y Pai, C Marvinney, A Said, T Yilmaz, Q Yin, C Gong, Z Tu, E Vescovo, *et al.*, “Observation of unconventional charge density wave without acoustic phonon anomaly in kagome superconductors av3sb5 (a= rb, cs),” arXiv preprint arXiv:2103.09769 (2021).
- [11] Yong Hu, Samuel ML Teicher, Brenden R Ortiz, Yang Luo, Shuting Peng, Linwei Huai, JZ Ma, NC Plumb, Stephen D Wilson, J-F He, *et al.*, “Charge-order-assisted topological surface states and flat bands in the kagome superconductor csv 3 sb 5,” arXiv preprint arXiv:2104.12725 (2021).
- [12] C. Mielke III au2, D. Das, J. X. Yin, H. Liu, R. Gupta, C. N. Wang, Y. X. Jiang, M. Medarde, X. Wu, H. C. Lei, J. J. Chang, P. Dai, Q. Si, H. Miao, R. Thomale, T. Neupert, Y. Shi, R. Khasanov, M. Z. Hasan, H. Luetkens, and Z. Guguchia, “Time-reversal symmetry-breaking charge order in a correlated kagome superconductor,” (2021), arXiv:2106.13443 [cond-mat.mtrl-sci].
- [13] Li Yu, Chennan Wang, Yuhang Zhang, Mathias Sander, Shunli Ni, Zouyouwei Lu, Sheng Ma, Zhengguo Wang, Zhen Zhao, Hui Chen, Kun Jiang, Yan Zhang, Haitao Yang, Fang Zhou, Xiaoli Dong, Steven L. Johnson, Michael J. Graf, Jiangping Hu, Hong-Jun Gao, and Zhongxian Zhao, “Evidence of a hidden flux phase in the topological kagome metal csv3sb5,” (2021), arXiv:2107.10714 [cond-mat.supr-con].
- [14] Qiong Wu, Z. X. Wang, Q. M. Liu, R. S. Li, S. X. Xu, Q. W. Yin, C. S. Gong, Z. J. Tu, H. C. Lei, T. Dong,

- and N. L. Wang, “The large static and pump-probe Kerr effect with two-fold rotation symmetry in kagome metal CsV_3Sb_5 ,” (2021), arXiv:2110.11306 [cond-mat.supr-con].
- [15] Shuo-Ying Yang, Yaojia Wang, Brenden R Ortiz, Defa Liu, Jacob Gayles, Elena Derunova, Rafael Gonzalez-Hernandez, Libor Šmejkal, Yulin Chen, Stuart SP Parkin, *et al.*, “Giant, unconventional anomalous hall effect in the metallic frustrated magnet candidate, Kv_3Sb_5 ,” *Science advances* **6**, eabb6003 (2020).
- [16] Hong Li, He Zhao, Brenden R. Ortiz, Takamori Park, Mengxing Ye, Leon Balents, Ziqiang Wang, Stephen D Wilson, and Ilija Zeljkovic, “Rotation symmetry breaking in the normal state of a kagome superconductor Kv_3Sb_5 ,” arXiv preprint arXiv:2104.08209 (2021).
- [17] Yuzki M. Oey, Brenden R. Ortiz, Farnaz Kaboudvand, Jonathan Frassinetti, Erick Garcia, Samuele Sanna, Vesna Mitrović, Ram Seshadri, and Stephen D. Wilson, “Fermi level tuning and double-dome superconductivity in the kagome metals $\text{CsV}_3\text{Sb}_{5-x}\text{Sn}_x$,” (2021), arXiv:2110.10912 [cond-mat.supr-con].
- [18] Shangfei Wu, Brenden R. Ortiz, Hengxin Tan, Stephen D. Wilson, Binghai Yan, Turan Birol, and Girsh Blumberg, “Charge density wave order in kagome metal av_3sb_5 ($a = \text{cs, rb, k}$),” (2022), arXiv:2201.05188 [cond-mat.str-el].
- [19] Hui Chen, Haitao Yang, Bin Hu, Zhen Zhao, Jie Yuan, Yuqing Xing, Guojian Qian, Zihao Huang, Geng Li, Yuhan Ye, *et al.*, “Roton pair density wave and unconventional strong-coupling superconductivity in a topological kagome metal,” arXiv preprint arXiv:2103.09188 (2021).
- [20] Linda Ye, Mingu Kang, Junwei Liu, Felix Von Cube, Christina R Wicker, Takehito Suzuki, Chris Jozwiak, Aaron Bostwick, Eli Rotenberg, David C Bell, *et al.*, “Massive Dirac fermions in a ferromagnetic kagome metal,” *Nature* **555**, 638–642 (2018).
- [21] Zhonghao Liu, Man Li, Qi Wang, Guangwei Wang, Chenhaoping Wen, Kun Jiang, Xianglu Lu, Shichao Yan, Yaobo Huang, Dawei Shen, *et al.*, “Orbital-selective Dirac fermions and extremely flat bands in frustrated kagome-lattice metal CoSn ,” *Nature communications* **11**, 1–7 (2020).
- [22] Zhiyong Lin, Jin-Ho Choi, Qiang Zhang, Wei Qin, Seho Yi, Pengdong Wang, Lin Li, Yifan Wang, Hui Zhang, Zhe Sun, *et al.*, “Flatbands and emergent ferromagnetic ordering in Fe_3Sn_2 kagome lattices,” *Physical review letters* **121**, 096401 (2018).
- [23] Enke Liu, Yan Sun, Nitesh Kumar, Lukas Muechler, Aili Sun, Lin Jiao, Shuo-Ying Yang, Defa Liu, Aiji Liang, Qianan Xu, *et al.*, “Giant anomalous Hall effect in a ferromagnetic kagome-lattice semimetal,” *Nature physics* **14**, 1125–1131 (2018).
- [24] M Yao, H Lee, N Xu, Y Wang, J Ma, OV Yazyev, Y Xiong, M Shi, G Aeppli, and Y Soh, “Switchable Weyl nodes in topological Kagome ferromagnet Fe_3Sn_2 ,” arXiv:1810.01514 (2018).
- [25] Mingu Kang, Linda Ye, Shiang Fang, Jih-Shih You, Abe Levitan, Minyong Han, Jorge I Facio, Chris Jozwiak, Aaron Bostwick, Eli Rotenberg, *et al.*, “Dirac fermions and flat bands in the ideal kagome metal FeSn ,” *Nature materials* **19**, 163–169 (2020).
- [26] Mingu Kang, Shiang Fang, Linda Ye, Hoi Chun Po, Jonathan Denlinger, Chris Jozwiak, Aaron Bostwick, Eli Rotenberg, Efthimos Kaxiras, Joseph G Checkelsky, *et al.*, “Topological flat bands in frustrated kagome lattice CoSn ,” *Nature communications* **11**, 1–9 (2020).
- [27] Hiroshi Watanabe and Nobuhiko Kunitomi, “On the neutron diffraction study of FeGe ,” *Journal of the Physical Society of Japan* **21**, 1932–1935 (1966).
- [28] Jia-Xin Yin, Yu-Xiao Jiang, Xiaokun Teng, Shafayat Hossain, Sougata Mardanya, Tay-Rong Chang, Zijin Ye, Gang Xu, Michael Denner, Titus Neupert, Benjamin Lienhard, Han-Bin Deng, Chandan Setty, Qimiao Si, Guoqing Chang, Zurab Guguchia, Bin Gao, Nana Shumiya, Qi Zhang, Tyler Cochran, Daniel Multer, Maksim Litskevich, Zi-Jia Cheng, Xian Yang, Ming Yi, Pengcheng Dai, and Zahid Hasan, “Microscopic evidence for topological charge order in kagome magnet FeGe ,” Submitted (2022).
- [29] M. Yi *et al.*, in preparation (2022).
- [30] Chandan Setty, Haoyu Hu, Lei Chen, and Qimiao Si, “Electron correlations and t -breaking density wave order in a \mathbb{Z}_2 kagome metal,” (2021), arXiv:2105.15204 [cond-mat.str-el].
- [31] Alexey A Soluyanov and David Vanderbilt, “Wannier representation of \mathbb{Z}_2 topological insulators,” *Physical Review B* **83**, 035108 (2011).
- [32] Alexey A Soluyanov and David Vanderbilt, “Smooth gauge for topological insulators,” *Physical Review B* **85**, 115415 (2012).
- [33] Nicola Marzari, Arash A Mostofi, Jonathan R Yates, Ivo Souza, and David Vanderbilt, “Maximally localized Wannier functions: Theory and applications,” *Reviews of Modern Physics* **84**, 1419 (2012).
- [34] Jan Kuneš, Ryotaro Arita, Philipp Wissgott, Alessandro Toschi, Hiroaki Ikeda, and Karsten Held, “Wien2wannier: From linearized augmented plane waves to maximally localized Wannier functions,” *Computer Physics Communications* **181**, 1888–1895 (2010).
- [35] Kristjan Haule, Chuck-Hou Yee, and Kyoo Kim, “Dynamical mean-field theory within the full-potential methods: Electronic structure of CeIrIn_5 , CeCoIn_5 , and CeRhIn_5 ,” *Physical Review B* **81**, 195107 (2010).
- [36] Peter Blaha, Karlheinz Schwarz, Fabien Tran, Robert Laskowski, Georg KH Madsen, and Laurence D Marks, “Wien2k: An APW+lo program for calculating the properties of solids,” *The Journal of Chemical Physics* **152**, 074101 (2020).
- [37] A key point to note, however, is that despite each pair of bands having a net Chern number zero, there is no guarantee that they form a *physical* elementary band representation (EBR). This is because despite the existence of exponentially localizable Wannier functions for pairs with $C = \pm 1$, the Wannier centers are off-site and break T -symmetry. This lack of adiabatic connectivity to the atomic limit renders the bands topological.

SUPPLEMENTAL MATERIAL

In this Supplemental Material, we further expand on the computational aspects of the electronic structure and edge state analysis.

Role of Coulomb interactions: Fig. 5 shows the DMFT DOS (top row) and spectral intensities (middle and bottom rows) as a function of increasing coulomb interaction U (columns from left to right correspond to $U = 4eV, 5eV, 6eV$ respectively). Many of the important low energy features such as location of the flat bands near E_f and Dirac cones remain intact with increasing correlations both with (bottom row) and without magnetic order (middle row). However, both the flat bands and Dirac cones at M become narrower and more localized as is natural when the electrons become strongly correlated. The spectral intensities are also suppressed indicating loss of quasiparticle-like behavior.

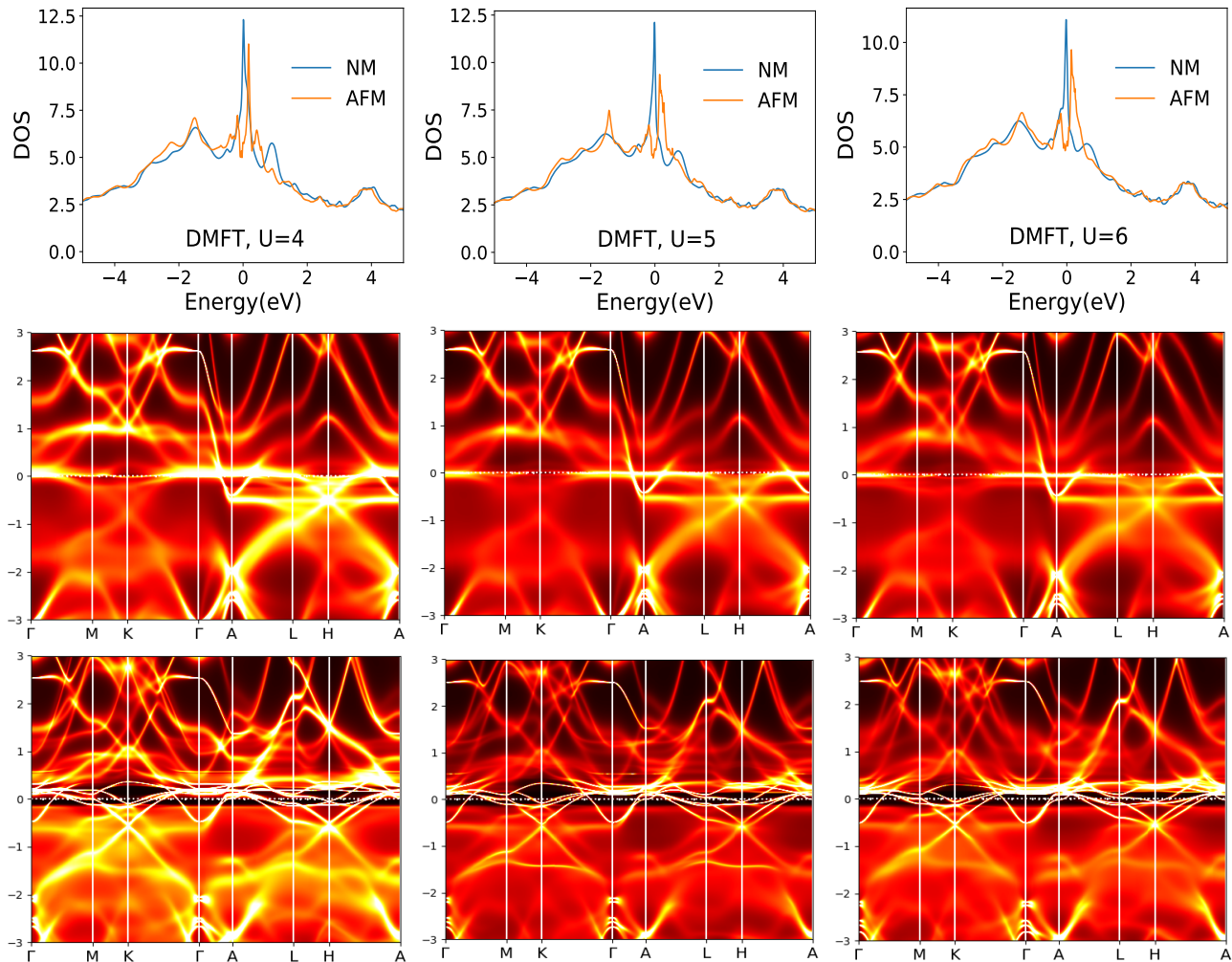


FIG. 5. Top row: DOS calculated from DMFT in the NM and magnetic phases. The plots are over a larger energy window than shown in the main text. (Middle row) DMFT bands with spectral intensities in the NM phase with SOC. (Bottom row) DMFT bands with spectral intensities in the magnetic phase with SOC. The columns from left to right correspond to $U = 4eV, 5eV, 6eV$ respectively.

Role of vHove singularities: Fig. 6 (left) marks different high intensity peaks and satellites features in the DOS and their relationship to various properties of the electronic structure. Fig. 6 (right) shows the same plot zoomed into a narrower energy window. Like in the main text, the short black arrows indicate peaks in the DOS that are determined by the flat bands. The long green arrow highlights the contribution from the vHove singularity. From a comparison of the relative intensities, it is evident that the role of vHove singularities is obscured by the more dominant flat band

effects. This is unlike the 135 ternary kagome compounds where the flat bands are buried deep below the fermi energy and vHove singularities have a greater influence on the low energy properties.

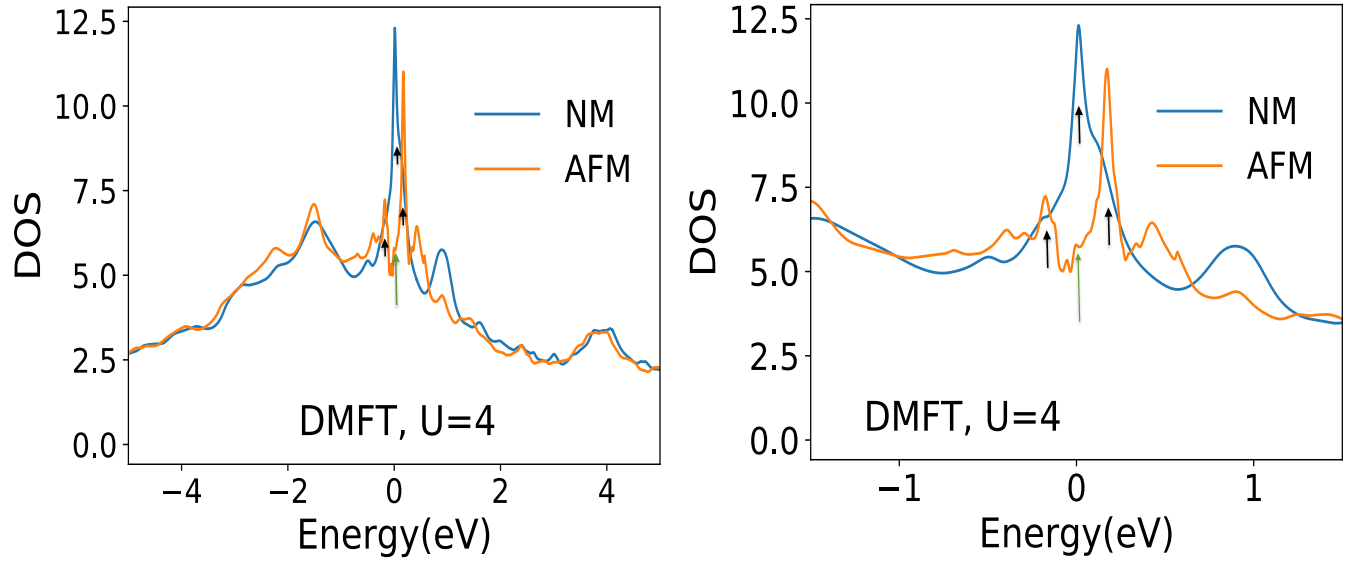


FIG. 6. Flat band vs vHove singularity contribution to the DOS in the NM and magnetic phases as calculated in DMFT. The black short arrows denote the dominant flat bands while the green long arrow denotes the v-Hove contribution. The right panel is a zoomed in version of the left for clarity.

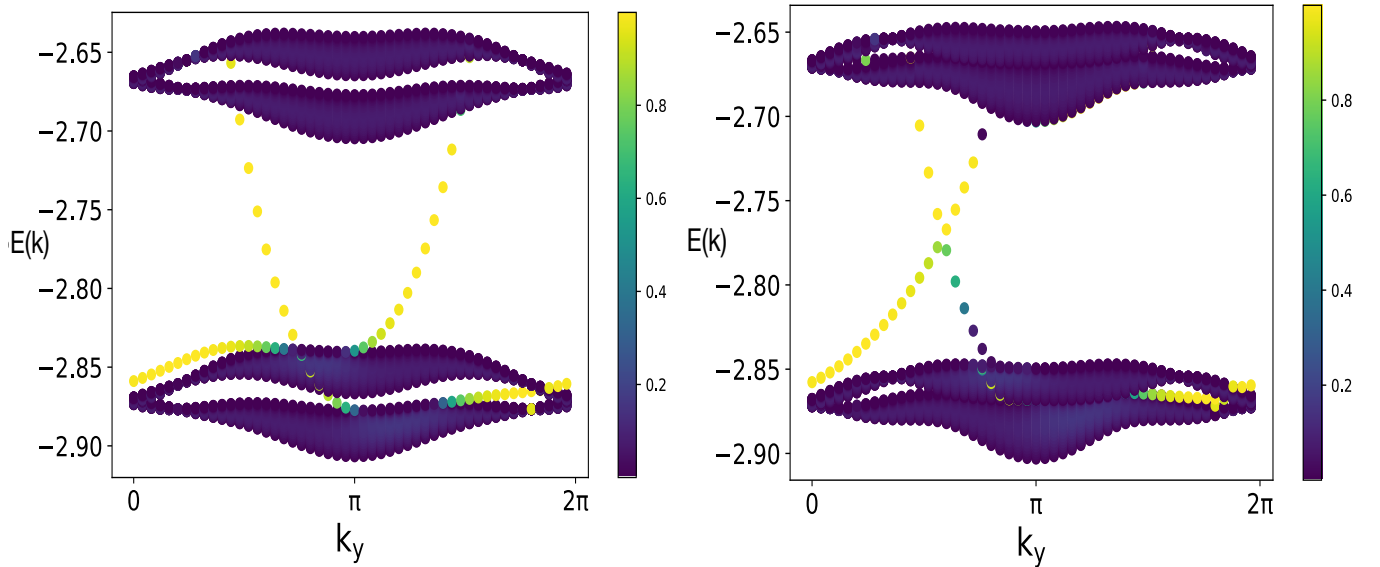


FIG. 7. Edge states in the charge order phase when the magnetic order is strong enough to fully gap out the bulk. The color scale marks the spectral weight of the states. In the left panel, the charge order parameter is comparable to the parent magnetic order. In the right panel, the charge order parameter is much smaller than the magnetic order parameter.

Large magnetic order: Here we consider the case where magnetic order completely polarizes the chern bands and gaps out the bulk at half filling. Fig. 7 (left) shows the edge states when the charge order parameter is comparable to the parent magnetic order. Edge states persist at both quarter filling and half filling. A similar scenario follows when the charge order parameter is much smaller than the magnetic order parameter (Fig. 7 (right)). However, note that in this scenario, the bulk state contribution to the STM DOS is non-existent at half filling. Whereas at quarter filling, there are both bulk and edge state contribution to the DOS.

Projected Hamiltonian in the Wannier basis: In this section, we derive the effective model in the Wannier basis. As shown in Ref. [30], the lowest two bands of the extended Hubbard model with Coulomb interaction on the kagome lattice can be projected into an effective Hamiltonian defined on the WOs. The projected creation and annihilation operators in the kagome lattice is connected with WOs with a sequence of unitary transformations:

$$Pc_{\mathbf{k}}P = \sum_{\mu} (V_{\mathbf{k}}^{\dagger}U_{H,\mathbf{k}})_{\mu\nu}b_{\mathbf{k}\nu}, \quad (7)$$

where $V_{\mathbf{k}}$ diagonalizes the hopping matrix, and $U_{H,\mathbf{k}}^{\dagger}$ is the Haldane matrix [32]. The kinetic part of effective Hamiltonian reads:

$$H_0 = \sum_{ij,\mu\nu} b_{i\mu}^{\dagger} t_{ij}^{\mu\nu} b_{j\nu}, \quad (8)$$

where

$$t_{ij}^{\mu\nu} = \sum_{\mu'\nu'i'j'} T_{i'j'}^{\mu'\nu'} \omega_{\mu'\mu,i'-i}^* \omega_{\nu'\nu,j'-j}, \quad (9)$$

with $\omega_{\alpha,\nu,i} = \frac{1}{N} \left(V_{\mathbf{k}}^{\dagger} U_{H,\mathbf{k}}^{\dagger} \right)_{\mu\nu} e^{i\mathbf{k}\cdot\mathbf{r}_i}$ the real space wave functions of the WOs.

The hopping parameters and the Zeeman field of the original kagome lattice are: $t_1 = 1$, $t_2 = -0.3$, $\lambda_1 = 0.28$, $\lambda_2 = 0.2$ and $h = 0.02$. We truncate the hoppings to the third nearest neighbor which are listed in Table. I, where μ/ν denote the orbitals and i/j denote the sites. To fix the particle number to be half-filled, we introduce the chemical potential $\mu = 0.067$. Fig. 8 shows a comparison between the bands of the original kagome lattice and the effective model.

(m, n)	(0, 1)	(1,0)	(1,1)	(m, n)	(0, 1)	(1,0)	(1,1)
$t_{m\mathbf{n}_1+n\mathbf{n}_2}^{00}$	-0.0007+i0.00319	-0.0007+i0.00319	0.0007-i0.00319	$t_{m\mathbf{n}_1+n\mathbf{n}_2}^{11}$	0.0007-i0.00319	0.0007-i0.00319	-0.0007+i0.00319
(m, n)	(2, 1)	(1,2)	(1,-1)	(m, n)	(2, 1)	(1,2)	(1,-1)
$t_{m\mathbf{n}_1+n\mathbf{n}_2}^{00}$	-0.003	-0.003	-0.003	$t_{m\mathbf{n}_1+n\mathbf{n}_2}^{11}$	-0.003	-0.003	-0.003
(m, n)	(0, 2)	(2,0)	(2, 2)	(m, n)	(0, 2)	(2,0)	(2, 2)
$t_{m\mathbf{n}_1+n\mathbf{n}_2}^{00}$	-0.0019-i0.00046	-0.0019-i0.00046	0.0019+i0.00046	$t_{m\mathbf{n}_1+n\mathbf{n}_2}^{11}$	0.0019+i0.00046	0.0019+i0.00046	-0.0019-i0.00046
(m, n)	(0, 0)	(0,1)	(-1, 0)	(m, n)	(0, 0)	(1,0)	(0, -1)
$t_{m\mathbf{n}_1+n\mathbf{n}_2}^{01}$	0.01	0.01	0.01	$t_{m\mathbf{n}_1+n\mathbf{n}_2}^{10}$	0.01	0.01	0.01
(m, n)	(1, -1)	(1,1)	(-1, -1)	(m, n)	(-1, 1)	(-1,-1)	(1, 1)
$t_{m\mathbf{n}_1+n\mathbf{n}_2}^{01}$	-0.0038	-0.0038	-0.0038	$t_{m\mathbf{n}_1+n\mathbf{n}_2}^{10}$	-0.0038	-0.0038	-0.0038

TABLE I. Table of hopping parameters of the effective Hamiltonian Eq. 3 appearing in the main text.

Ginzburg-Landau (GL) free energy: The GL free energy to fourth order in perturbation is given by

$$\begin{aligned}
F[\Delta_{\mathbf{Q}_i}] &= \alpha \sum_i |\Delta_{\mathbf{Q}_i}|^2 + \beta_1 \sum_i |\Delta_{\mathbf{Q}_i}|^4 \\
&+ \beta_2 \sum_{i<j} |\Delta_{\mathbf{Q}_i}|^2 |\Delta_{\mathbf{Q}_j}|^2 - h'\gamma \sum_i \Delta_{\mathbf{Q}_i} \Delta_{-\mathbf{Q}_i} \\
&+ \alpha' \sum_i |\Delta'_{\mathbf{Q}_i}|^2 + \beta'_1 \sum_i |\Delta'_{\mathbf{Q}_i}|^4 \\
&+ \beta'_2 \sum_{i<j} |\Delta'_{\mathbf{Q}_i}|^2 |\Delta'_{\mathbf{Q}_j}|^2 - h'\gamma \sum_i \Delta'_{\mathbf{Q}_i} \Delta'_{-\mathbf{Q}_i} \\
&+ \dots \quad .
\end{aligned} \quad (10)$$

Here the parameters $\alpha, \alpha', \beta_i, \beta'_i, \gamma$ are constants that depend on details of the electronic structure. The expression for γ in the flat band limit is given as

$$\gamma = \sum_{k_n} \frac{6h_0}{(h_0^2 + k_n^2)^2}. \quad (11)$$

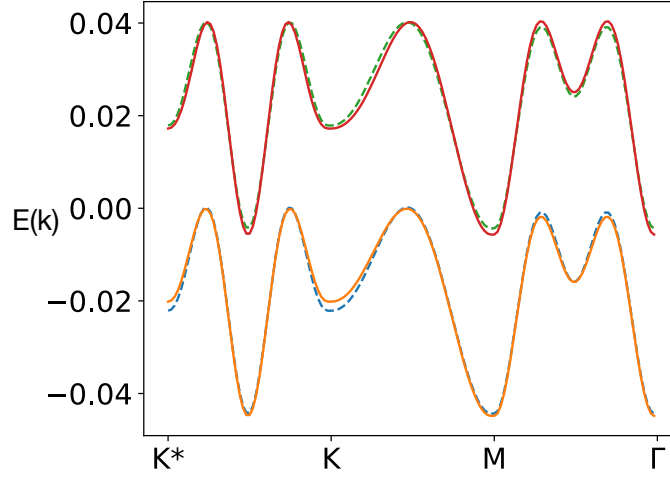


FIG. 8. Comparison of dispersions along high symmetry lines of the lowest degenerate doublet of kagome bands. Dashed line is the original kagome band and solid line is from the effective model with WOs.

where k_n is the Fermionic Matsubara frequency and h_0 is the static external field. The Matsubara sum can be evaluated to give

$$\gamma \simeq \frac{3h_0}{2T_{CO}^4} \left[\frac{-1 + \tilde{h}_0^{-1} \sinh \tilde{h}_0}{\tilde{h}_0^2 (1 + \cosh \tilde{h}_0)} \right] \quad (12)$$

$$\tilde{h}_0 \equiv h_0/T_{CO}. \quad (13)$$

This expression for γ is used in the main text of the Hamiltonian.

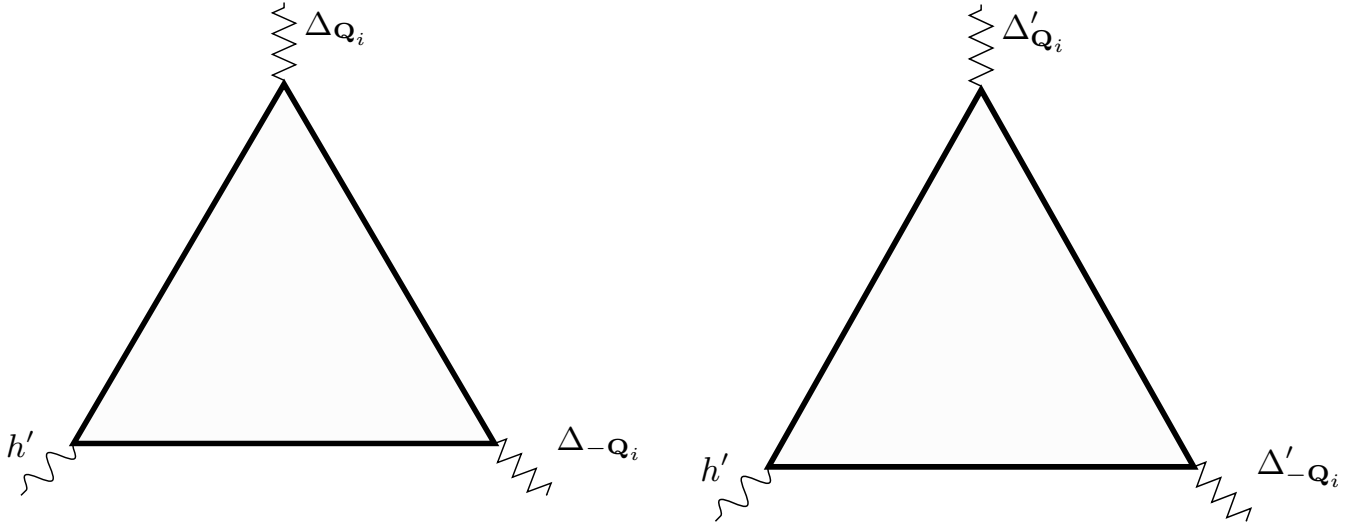


FIG. 9. Lowest order Feynman diagrams that couple the charge order fluctuations $\Delta_{\mathbf{Q}_i}$ and $\Delta'_{\mathbf{Q}_i}$ (zig-zag lines) to fluctuations of the broken time reversal field (wavy lines) h' . The solid lines are the electron Green functions in a static external field h_0 . These terms drive the enhanced magnetic moment in the charge order phase.